Low Temperature Physics/Fizika Nizkikh Temperatur, 2018, v. 44, No. 12, pp. 1606–1617

Quantum discretization of Landau damping

S.G. Castillo-López and F. Pérez-Rodríguez

Instituto de Física, Benemérita Universidad Autónoma de Puebla, Puebla, Pue. 72570, México

N.M. Makarov

Instituto de Ciencias, Benemérita Universidad Autónoma de Puebla, Puebla, Pue., 72570, México
E-mail: nykolay.makarov@correo.buap.mx; makarov.n@gmail.com

Received July 3, 2018, published online October 26, 2018

We derive and analyze analytical expressions for the quantum electron current density and electromagnetic field distribution inside a metallic nanoslab. Besides, we obtain general explicit expressions for the surface impedances of both metal slab boundaries. We found that the phenomenon of Landau damping manifests itself in the frequency dependence of the surface impedances as resonances associated with the discretization of the electromagnetic and electron wave numbers inside the metal nanoslab. In particular, the quantum nonlocal resonances of the surface impedances are clearly discernible at slab thicknesses smaller than the electromagnetic skin depth. The predictions for the surface impedances in the quantum regime turn out to be radically different from those of the quantum local approach, the semiclassical Boltzmann kinetic equation formalism and the classical Drude–Lorentz local model. The analytical study completely agrees with the respective numerical calculations.

Keywords: spatial dispersion, Landau damping, metallic nanostructures, optical properties.

1. Introduction

As is well known (see, i.e., Ref. 1), there are three principal mechanisms of electromagnetic absorption in metals: The first one is owing to the collisions of electrons in the sample, it is characterized by a relaxation frequency ν; the second mechanism is also collisional, but it is connected with the dissipative properties of a metallic surface and is described by a surface relaxation frequency ν_{surf}; the third mechanism turns out to be collisionless and is known as Landau damping [2]. The latter one describes the phenomenon of direct absorption of electromagnetic radiation by the electrons moving in phase with the electromagnetic wave. Therefore, in metallic samples of very high quality and at sufficiently low temperatures, the remaining mechanism of electromagnetic absorption is, precisely, the Landau damping. This phenomenon is well manifested under conditions of strong spatial dispersion, or nonlocality, of the metal. Particularly, it has been studied in bulk samples (see, for example, [1] and references therein), thin films [3] and metal-dielectric periodic heterostructures [4–6] within the framework of the semiclassical formalism of the Boltzmann kinetic equation for the distribution function of the conduction electrons. As was shown there, Landau damping always exists and considerably alters the absorption, reflection and transmission spectra of all those metal systems within the THz and near-infrared frequency range. Landau damping also influences upon optical spectra in the visible and ultraviolet ranges. Thus, for example, it contributes to the attenuation of surface plasmons in a great variety of metallic nanostructures (see, e.g., [7–16]). However, because of the extremely-small size of the metallic samples (nano-thin films, nanotubes, and nanoparticles), the quantum phenomena emerge and the question about the physical interpretation of the classical phenomenon of Landau damping in the strong quantum regime arises. Clarifying this question, in our recently-published brief letter [17], the resonant quantization of Landau damping in far-infrared absorption spectra of metal nano-thin films was predicted within the Kubo formalism. It was demonstrated that Landau damping clearly manifests itself as prominent resonances in the absorption spectra, which are associated with the discretization of the electromagnetic and electron wave numbers inside a metal nanofilm.

In this work we shall present a detailed analysis of the quantum nonlocal electromagnetic response of a metal nanoslab and, particularly, we study the effect of Landau damping on it. Firstly (Sec. 2), we shall analytically calculate the quantum current density of the conduction electrons in the metal nanoslab by applying the Kubo's linear response formalism. Using this analytical result, we solve Maxwell equations by writing the electromagnetic field as

a superposition of discrete normal electromagnetic modes with quantized electromagnetic wave vector (Sec. 3). In Sec. 4, we obtain explicit expressions for the surface impedances of both boundaries of the nanoslab in order to study its external response. Here, from the general expressions for the surface impedances we derive asymptotic formulas for three limits of the electromagnetic response of the metal nanoslab: i) the quantum local regime, ii) the semiclassical nonlocal limit, which can also be described by the Boltzmann kinetic equation formalism, and iii) the regime corresponding to the classical Drude–Lorentz local approach. The Sec. 5 contains specific results obtained by numerical calculations of the surface impedances of silver nanoslabs having distinct thicknesses. On the basis of both analytical and numerical results, we shall explain the resonances, appearing in the frequency dependence of the surface impedances in the quantum regime, as an effect of the quantum discretization of the Landau damping. Finally, there is a section of Conclusions.

2. Problem formulation: basic relations

We examine an electromagnetic response of a quantum metallic flat layer confined to the space volume

$$0 \leqslant x \leqslant d, \qquad -\infty < y,z < \infty, \tag{2.1}$$

with d implying the slab thickness. The coordinate system is chosen in such a way that the x axis is orthogonal to the layer interfaces $x = 0$ and $x = d$ while the y and z axes are parallel to them being found on the left metal boundary $x = 0$, see Fig. 1.

The single-particle quantum stationary states of the conduction electrons in the metal slab (2.1), unperturbed by the electromagnetic field, are characterized by the complete set a consisting of three electron quantum numbers,

$$a = \{n, q_y, q_z\}, \quad n = 1, 2, 3, \ldots; \; -\infty < q_y, q_z < \infty. \tag{2.2}$$

The positive integer n determines the discrete electron wave number q_x transversal to the metal slab,

$$q_x = q_n \equiv \pi n/d. \tag{2.3}$$

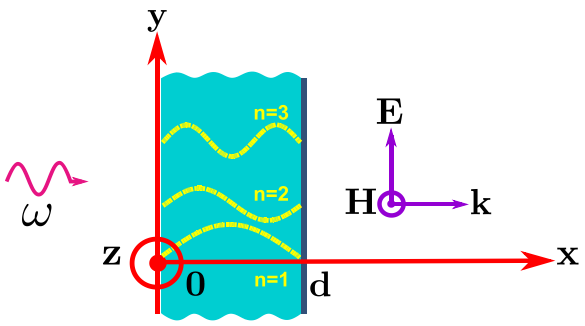

Fig. 1. Sketch of the system.

Two other, longitudinal, wave numbers, q_y and q_z, are continuous quantities because of the free unconfined electron motion along y and z axes.

The dependence of the eigenenergy ϵ_a of the unperturbed electron Hamiltonian on the quantum numbers (2.2) is defined by

$$\epsilon_a = \epsilon_n(q_y, q_z) \equiv \frac{\hbar^2}{2m}(q_n^2 + q_y^2 + q_z^2), \tag{2.4}$$

with m being the effective electron mass. The orthonormalized wave function of the electron in the a-state inside the metal layer reads

$$\Psi_a(x,y,z) = \sqrt{\frac{2}{d}} \sin(q_n x) \frac{1}{2\pi} \exp(iq_y y + iq_z z). \tag{2.5}$$

For simplicity, we assume the specular reflection of electrons from the metal slab boundaries $x = 0$ and $x = d$.

The exciting electromagnetic wave of frequency ω propagates along the x axis perpendicularly to the metal layer. In view of the chosen coordinate system, this fact implies the electric $\mathbf{E}(x,t)$ and magnetic $\mathbf{H}(x,t)$ fields of the wave to be parallel to the y and z axis, respectively,

$$\mathbf{E}(x,t) = \{0, E(x), 0\} \exp(-i\omega t), \tag{2.6a}$$

$$\mathbf{H}(x,t) = \{0, 0, H(x)\} \exp(-i\omega t). \tag{2.6b}$$

From the Maxwell equations one can readily obtain the equation, which describes the electric field distribution inside the metal slab (2.1),

$$\frac{d^2E(x)}{dx^2} + k^2 E(x) + \frac{4\pi i k^2}{\omega} j(x) = 0. \tag{2.7}$$

Here $k = \omega/c$ is the electromagnetic wave number in vacuum, the second term on the l.h.s. is originated from the displacement current, while the third one is due to the longitudinal current density $j(x)\exp(-i\omega t)$ of the conduction electrons. The magnetic field $H(x)$ is associated with the derivative $E'(x)$ over x of the electric field $E(x)$ by the Faraday law,

$$E'(x) = ikH(x). \tag{2.8}$$

The quantum current density of the conduction electrons, $\mathbf{j}(x,\mathbf{r};t) = \mathbf{j}(x,\mathbf{r})\exp(-i\omega t)$, in linear approximation in the electric field $\mathbf{E}(x,\mathbf{r};t) = \mathbf{E}(x,\mathbf{r})\exp(-i\omega t)$ can be derived with employing the standard Kubo's linear response theory developed for the weakly nonequilibrium isotropic Fermi-liquid model [18–20]. Thus, the starting point of our calculations is the general expression [21]

$$j_\alpha(x,\mathbf{r}) = \int_V dx' d^2\mathbf{r}' \chi_{\alpha\beta}(x,\mathbf{r};x',\mathbf{r}') E_\beta(x',\mathbf{r}'); \tag{2.9}$$

$$\alpha, \beta = x, y, z; \quad \mathbf{r} = \{y, z\};$$

where the integration runs over the metal volume V, see Eq. (2.1), and the summation over the twice-repeated vector index β is implied. The response function $\chi_{\alpha\beta}$ is defined as

$$\chi_{\alpha\beta}(x,\mathbf{r};x',\mathbf{r}') = 2\hbar \sum_{a,a'} \frac{\mathfrak{F}_a - \mathfrak{F}_{a'}}{\epsilon_{a'} - \epsilon_a} \times$$

$$\times \frac{\langle a \,|\, I_\alpha(x,\mathbf{r}) \,|\, a' \rangle \langle a' \,|\, I_\beta(x',\mathbf{r}') \,|\, a \rangle}{\hbar\nu + i(\epsilon_{a'} - \epsilon_a - \hbar\omega)}. \qquad (2.10)$$

Here the factor 2 takes into account the electron spin degeneration, the symbols a and a' stand for the complete set (2.2), (2.3) of the quantum numbers of the unperturbed electron state with the corresponding eigenenergies ϵ_a and $\epsilon_{a'}$, Eq. (2.4). The sum-symbol implies summation over discrete quantum numbers and integration over continuous ones. The equilibrium Fermi distribution function $\mathfrak{F}_a$ at the energy $\epsilon = \epsilon_a$, the Fermi energy ϵ_F and the temperature T is

$$\mathfrak{F}_a = \left\{1 + \exp[(\epsilon_a - \epsilon_F)/T]\right\}^{-1}. \qquad (2.11)$$

The so-called adiabatic parameter ν can be regarded as the effective scattering frequency of electrons caused by their collisions with scatters in metal. Then,

$$\langle a \,|\, I_\alpha(x,\mathbf{r}) \,|\, a' \rangle = \frac{i\hbar e}{2m} [\Psi^*_a(x,\mathbf{r}) \nabla_\alpha \Psi_{a'}(x,\mathbf{r}) -$$

$$- \Psi_{a'}(x,\mathbf{r}) \nabla_\alpha \Psi^*_a(x,\mathbf{r})] \qquad (2.12)$$

is the matrix element of the α-th component of the current-density operator, where the asterisk "*" means the complex conjugation, e is the elementary charge, and $\Psi_a(x,\mathbf{r})$ stands for the unperturbed wave function (2.5) of the electron in the α-th stationary state.

Since the electromagnetic field (2.6) does not depend on the radius-vector $\mathbf{r} = \{y,z\}$, the electron current density $\mathbf{j}(x,\mathbf{r};t)$ should also be independent of $\mathbf{r} = \{y,z\}$. In addition, it has the same polarization as the electric field (2.6a),

$$\mathbf{j}(x,\mathbf{r};t) = \{0, j(x), 0\} \exp(-i\omega t). \qquad (2.13)$$

In line with the general relation (2.9) one can readily obtain

$$j(x) = \int_0^d dx' \chi(x,x') E(x'), \quad 0 \leqslant x \leqslant d, \qquad (2.14)$$

where the truncated response function $\chi(x,x')$ is described by

$$\chi(x,x') = \int_{-\infty}^{\infty} d^2\mathbf{r}' \chi_{yy}(x,\mathbf{r};x',\mathbf{r}'). \qquad (2.15)$$

By definition (2.12), the necessary matrix elements get the following explicit expressions:

$$\langle a \,|\, I_y(x,\mathbf{r}) \,|\, a' \rangle = -\frac{\hbar e(q_y + q'_y)}{md(2\pi)^2} \sin(q_n x) \sin(q_{n'} x) \times$$

$$\times \exp[-i(q_y - q'_y)y] \exp[-i(q_z - q'_z)z], \qquad (2.16a)$$

$$\langle a' \,|\, I_y(x',\mathbf{r}') \,|\, a \rangle = -\frac{\hbar e(q_y + q'_y)}{md(2\pi)^2} \sin(q_n x') \sin(q_{n'} x') \times$$

$$\times \exp[i(q_y - q'_y)y'] \exp[i(q_z - q'_z)z']. \qquad (2.16b)$$

Being substituted into Eq. (2.10), they allow us to take the integral over $\mathbf{r}' = \{y',z'\}$ contained in Eq. (2.15), giving rise to the appearance of two Dirac delta-functions, $\delta(q_y - q'_y)$ and $\delta(q_z - q'_z)$. Using them, one can explicitly take the integrals over q'_y and q'_z entering the sum-symbol over a' in Eq. (2.10) and eliminate the dependence on the radius-vector $\mathbf{r} = \{y,z\}$. As a result, we get the exact explicit quantum expression for $\chi(x,x')$,

$$\chi(x,x') = \frac{2\hbar^2 e^2}{m^2} \sum_{n,n'=1}^{\infty} \int_{-\infty}^{\infty} \frac{dq_z}{2\pi} \int_{-\infty}^{\infty} \frac{dq_y}{2\pi} q_y^2 \times$$

$$\times \frac{\mathfrak{F}_n(q_y,q_z) - \mathfrak{F}_{n'}(q_y,q_z)}{\epsilon_{n'}(q_y,q_z) - \epsilon_n(q_y,q_z)} \times \qquad (2.17)$$

$$\times \frac{(2/d)^2 \sin(q_n x) \sin(q_{n'} x) \sin(q_n x') \sin(q_{n'} x')}{(\nu - i\omega) + i\hbar(q_{n'}^2 - q_n^2)/2m}.$$

It is important to emphasize that the truncated response function (2.17) is even and periodic one of period $2d$ with respect to its arguments x and x',

$$\chi(x,x') = \chi(-x,x') = \chi(x,-x'),$$

$$\chi(x,x') = \chi(x+2d,x') = \chi(x,x'+2d). \qquad (2.18)$$

The noted symmetries provide the adequate and physically reasonable type of the Fourier presentation in order to proceed further resolving the problem.

3. Discrete electromagnetic modes

Equation (2.7) with the current density $j(x)$ determined by Eqs. (2.14), (2.17), presents an integro-differential equation for $E(x)$, which is defined within the finite interval $0 \leqslant x \leqslant d$. Due to symmetries (2.18), we can try to solve it by passing to the discrete Fourier transformations similarly as we did this in the classical case, see Ref. 3.

Specifically, the electric current density $j(x)$ defined inside the finite interval $0 \leqslant x \leqslant d$, on the other hand, is an even and periodic function of x in accordance with Eqs. (2.14), (2.18),

$$j(x) = j(-x); \quad j(x) = j(x+2d). \qquad (3.1a)$$

This parity-periodicity symmetry analytically continues $j(x)$ to the entire x axis $(-\infty < x < \infty)$. The electric field

$E(x)$ in metal slab is also defined within the finite interval $0 \leqslant x \leqslant d$. However, the connection $E(x)$ with $j(x)$ via Eq. (2.7), makes the former to be even and periodic too,

$$E(x) = E(-x); \quad E(x) = E(x+2d), \tag{3.1b}$$

that analytically continues the electric field $E(x)$ to the entire x axis $(-\infty < x < \infty)$.

The parity-periodicity symmetry (3.1) inevitably dictates the following Fourier transformations with the discrete electromagnetic wave number

$$k_s = \pi s/d, \quad s = 0, \pm 1, \pm 2, \pm 3, \ldots. \tag{3.2}$$

For the electric field we introduce

$$E(x) = \frac{1}{2d} \sum_{s=-\infty}^{\infty} \mathcal{E}(k_s) \cos(k_s x), \tag{3.3a}$$

$$\mathcal{E}(k_s) = 2\int_0^d dx E(x) \cos(k_s x). \tag{3.3b}$$

The similar for the electric current density

$$j(x) = \frac{1}{2d} \sum_{s=-\infty}^{\infty} j(k_s) \cos(k_s x), \tag{3.4a}$$

$$j(k_s) = 2\int_0^d dx\, j(x) \cos(k_s x). \tag{3.4b}$$

By definitions (3.3b) and (3.4b), the Fourier transforms $\mathcal{E}(k_s)$ and $j(k_s)$ are even functions of the electromagnetic wave number k_s,

$$\mathcal{E}(k_s) = \mathcal{E}(-k_s) = \mathcal{E}(k_{-s}); \tag{3.5a}$$

$$j(k_s) = j(-k_s) = j(k_{-s}). \tag{3.5b}$$

Now, let us apply the integral operator

$$2\int_0^d dx \cos(k_s x) \ldots \tag{3.6}$$

to Eq. (2.7) with subsequent double integration by parts of the first (differential) term. After that, the initial equation (2.7) in k_S-representation gets the form

$$\left\{k_s^2 - k^2\right\} \mathcal{E}(k_s) - \frac{4\pi i k^2}{\omega} j(k_s) =$$

$$= 2ik[H(d)\cos(k_s d) - H(0)]. \tag{3.7}$$

The integration constants $H(0)$ and $H(d)$ are the magnetic fields on the metal slab surfaces $x = 0$ and $x = d$. They are associated, respectively, with the derivatives $E'(0)$ and $E'(d)$ of the electric field by the Maxwell equation (2.8). Depending on the method of the slab excitation, $H(0)$ and $H(d)$ can be expressed via the amplitudes of the incident, reflected and transmitted waves with the use of continuity conditions for the electric and magnetic fields at the $x = 0$ and $x = d$ boundaries.

In order to derive $j(k_s)$ we have to Fourier transform Eq. (2.14) for the current density $j(x)$ as stated in definition (3.4b),

$$j(k_s) = 2\int_0^d dx' E(x') \int_0^d dx \chi(x, x') \cos(k_s x). \tag{3.8}$$

Substitution of Eq. (2.17) for the truncated response function $\chi(x, x')$ into Eq. (3.8) gives

$$j(k_s) = \frac{\hbar^2 e^2}{4m^2 d} \sum_{n,n'=-\infty}^{\infty} \int_{-\infty}^{\infty} \frac{dq_z}{2\pi} \int_{-\infty}^{\infty} \frac{dq_y}{2\pi} q_y^2 \times$$

$$\times \frac{\mathfrak{F}_n(q_y, q_z) - \mathfrak{F}_{n'}(q_y, q_z)}{\epsilon_{n'}(q_y, q_z) - \epsilon_n(q_y, q_z)} \left[(\nu - i\omega) + \frac{i\hbar}{2m}(q_{n'}^2 - q_n^2)\right]^{-1} \times$$

$$\times 4\int_0^d dx' E(x') \sin(q_n x') \sin(q_{n'} x') \times$$

$$\times \frac{4}{d} \int_0^d dx \cos(k_s x) \sin(q_n x) \sin(q_{n'} x). \tag{3.9}$$

Here we have taken into account that the summand in Eq. (2.17) is an even function of the summation indices n and n'. Then, the summand vanishes as $n = 0$, or $n' = 0$. These facts allowed us to make a helpful replacement,

$$\sum_{n,n'=1}^{\infty} \ldots \quad \rightarrow \quad \frac{1}{4} \sum_{n,n'=-\infty}^{\infty} \ldots. \tag{3.10}$$

Following definition (3.3b) and known integral expression for the Kronecker delta-symbol $\delta_{s,s'}$, it is readily to realize that

$$4\int_0^d dx' E(x') \sin(q_n x') \sin(q_{n'} x') =$$

$$= \mathcal{E}(q_n - q_{n'}) - \mathcal{E}(q_n + q_{n'}); \tag{3.11a}$$

$$\frac{4}{d}\int_0^d dx \cos(k_s x) \sin(q_n x) \sin(q_{n'} x) =$$

$$= \delta_{n',n+|s|} + \delta_{n',n-|s|} - \delta_{-n',n+|s|} - \delta_{-n',n-|s|}. \tag{3.11b}$$

Substitute Eqs. (3.11) into Eq. (3.9). Then, in the third and fourth terms, containing, respectively, $\delta_{-n',n+|s|}$ and $\delta_{-n',n-|s|}$ change the summation index, $n' \rightarrow -n'$. As a result, the third and fourth terms turn into the first and the second ones. So, we obtain

$$j(k_s) = \frac{\hbar^2 e^2}{2m^2 d} \sum_{n,n'=-\infty}^{\infty} \int_{-\infty}^{\infty} \frac{dq_z}{2\pi} \int_{-\infty}^{\infty} \frac{dq_y}{2\pi} q_y^2 \times$$

$$\times \frac{\mathfrak{F}_n(q_y,q_z)-\mathfrak{F}_{n'}(q_y,q_z)}{\epsilon_{n'}(q_y,q_z)-\epsilon_n(q_y,q_z)}\left[(\nu-i\omega)+\frac{i\hbar}{2m}(q_{n'}^2-q_n^2)\right]^{-1}\times$$

$$\times\left[\mathcal{E}(q_n-q_{n'})-\mathcal{E}(q_n+q_{n'})\right](\delta_{n',n+|s|}+\delta_{n',n-|s|}). \quad (3.12)$$

Now, carry out double replacement of the summation indices, $n\to -n$ and $n'\to -n'$, in the second term with $\delta_{n',n-|s|}$. This operation transforms $\delta_{n',n+|s|}+\delta_{n',n-|s|}\to$ $\to 2\delta_{n',n+|s|}$. Perform the summation over n' with the use of the Kronecker delta $\delta_{n',n+|s|}$. All this algebra yields

$$j(k_s)=\frac{i\hbar^2e^2}{m^2d}\sum_{n=-\infty}^{\infty}\int_{-\infty}^{\infty}\frac{dq_z}{2\pi}\int_{-\infty}^{\infty}\frac{dq_y}{2\pi}q_y^2\times$$

$$\times\frac{\mathfrak{F}_n(q_y,q_z)-\mathfrak{F}_{n+|s|}(q_y,q_z)}{\epsilon_{n+|s|}(q_y,q_z)-\epsilon_n(q_y,q_z)}\times$$

$$\times\frac{\mathcal{E}(k_s)-\mathcal{E}(|k_s|+2q_n)}{\omega-\omega_{n+|s|,n}+i\nu}. \quad (3.13)$$

When accomplishing the above calculations, we have applied the evenness of the quantum electron energy (2.4) as a function of the discrete quantum number n, the evenness of the electric field Fourier transform (3.5a), and the evident conservation law for the discrete transverse electron wave-number q_n,

$$q_{n+|s|}=q_n+|k_s|. \quad (3.14)$$

Additionally, in Eq. (3.13) we have introduced the quantum frequency $\omega_{n+|s|,n}$ of electron transition between (n + |s|)-th and n-th energy levels (2.4) because of absorption or emission of the electromagnetic quantum $\hbar|k_s|$,

$$\omega_{n+|s|,n}=\frac{\hbar}{2m}\left(q_{n+|s|}^2-q_n^2\right)=\omega_{n,s}+\omega_s; \quad (3.15a)$$

$$\omega_{n,s}=\frac{\hbar|k_s|q_n}{m}=|k_s|V_F\frac{q_n}{k_F},\quad \omega_s=\frac{\hbar k_s^2}{2m}, \quad (3.15b)$$

with $V_F=\sqrt{2\epsilon_F/m}$ and $k_F=\sqrt{2m\epsilon_F}/\hbar$ being the electron Fermi velocity and the electron Fermi wave number, respectively. Note that $\omega_{-n-|s|,-n}=\omega_{n+|s|,n}$. The quantum transition frequency (3.15a) consists of two terms: $\omega_{n,s}$ represents the quasi-classical version of $\omega_{n+|s|,n}$, whereas ω_s is known as the recoil frequency that cannot be introduced within the quasi-classical approximation. Since ω_s does not have a classical counterpart, it should be omitted when passing to the classical limit.

Further simplification of Eq. (3.13) is provided with the relation

$$\frac{\mathfrak{F}_n(q_y,q_z)-\mathfrak{F}_{n+|s|}(q_y,q_z)}{\epsilon_{n+|s|}(q_y,q_z)-\epsilon_n(q_y,q_z)}\approx\delta(\epsilon_n(q_y,q_z)-\epsilon_F)=$$

$$=\frac{2m}{\hbar^2}\delta(q_y^2+q_z^2-[k_F^2-q_n^2]). \quad (3.16)$$

The Dirac delta-function describes the energy conservation law, which holds true in metallic solid-state media whose temperature is always much smaller than the electron Fermi energy, $T\ll\epsilon_F$. Note that the main temperature dependence of the metal conductivity is originated from the collisional relaxation rate ν of conduction electrons. Therefore,

$$j(k_s)=\frac{ie^2}{\pi^2md}\sum_{n=-\infty}^{\infty}\frac{\mathcal{E}(k_s)-\mathcal{E}(|k_s|+2q_n)}{\omega-\omega_{n+|s|,n}+i\nu}I_n, \quad (3.17)$$

where the integral I_n is defined by

$$I_n=2\int_0^{\infty}dq_z\int_0^{\infty}dq_y\,q_y^2\delta(q_y^2+q_z^2-[k_F^2-q_n^2]). \quad (3.18)$$

Deriving the integral (3.18), we pass to the polar coordinates, $q_y=q_t\cos\varphi$, $q_z=q_t\sin\varphi$, $dq_ydq_z=q_tdq_td\varphi$. Then,

$$I_n=2\int_0^{\infty}dq_t\,q_t^3\delta(q_t^2-[k_F^2-q_n^2])\int_0^{\pi/2}d\varphi\cos^2\varphi=$$

$$=\begin{cases}\dfrac{\pi}{4}(k_F^2-q_n^2) & \text{for}\quad |q_n|=\pi|n|/d<k_F,\\ 0 & \text{otherwise.}\end{cases} \quad (3.19)$$

Remarkably, Eq. (3.19) being substituted into Eq. (3.17), confines the variation of the summation index n to the finite interval $-N_F\leqslant n\leqslant N_F$, where

$$N_F=[k_Fd/\pi]. \quad (3.20)$$

The number N_F is called total number of electron conducting channels in a metal slab of thickness d. It is defined by the integer part $[k_Fd/\pi]$ of the channel parameter k_Fd/π. Because of quantization (2.3) of the electron transverse wave number $q_x=q_n$ with simultaneous conservation of the electron energy $\epsilon_n(q_t)=\epsilon_F$, the wave number q_t of the longitudinal wave vector $\mathbf{q}_t=\{q_y,q_z\}$ is also quantized, $q_t=\sqrt{k_F^2-q_n^2}$. Evidently, the electron transport inside a metal slab is provided only by quantum states that can propagate along the slab, i.e., have a real values of the longitudinal wave number q_t. This means that the quantum index $|n|$ of such a propagating state, or conducting channel, is restricted by N_F. All other electron states with indices $|n|>N_F$ are known as evanescent since they have purely imaginary values of q_t and, consequently, do not contribute to the electron transport properties.

Thus, the final expression for the Fourier transform $j(k_s)$ of the electron current density $j(x)$ reads

$$j(k_s)=\frac{3i\omega_p^2}{16\pi}\left(\frac{k_F d}{\pi}\right)^{-1}\sum_{n=-N_F}^{N_F}\left(1-\frac{q_n^2}{k_F^2}\right)\times$$

$$\times\frac{\mathcal{E}(k_s)-\mathcal{E}(|\,k_s\,|+2q_n)}{\omega-\omega_{n+|s|,n}+i\nu}. \qquad (3.21)$$

Here ω_p is the plasma frequency,

$$\omega_p^2=4\pi Ne^2/m, \qquad N=k_F^3/3\pi^2, \qquad (3.22)$$

and N is the classical density of the gas of conduction electrons in a bulk metal.

The quantum current density (3.21) contains both diagonal and off-diagonal terms proportional to $\mathcal{E}(k_s)$ and $\mathcal{E}(|\,k_s\,|+2q_n)$, respectively. As a consequence, the substitution of Eq. (3.21) into Eq. (3.7) turns the latter into a set of equations that cannot give rise to relatively simple and easily appreciated (recognized) results. At the same time, the respective numerical simulations show that the principal contribution to Eq. (3.21) is provided by the diagonal part only. Therefore, to proceed further analytically, we omit the rapidly oscillating term with $\mathcal{E}(|\,k_s\,|+2q_n)$. Following definition (3.3a) and the Faraday law (2.8), such a model allows us to readily obtain the compact and physically reasonable expressions for the electric and magnetic fields inside the metal slab (2.1), $0\leqslant x\leqslant d$,

$$E(x)=\frac{ik}{d}\sum_{s=-\infty}^{\infty}\frac{H(d)\cos\left[k_s(d-x)\right]-H(0)\cos(k_s x)}{k_s^2-k^2\varepsilon(k_s)}, \qquad (3.23a)$$

$$H(x)=\frac{1}{d}\sum_{s=-\infty}^{\infty}k_s\frac{H(d)\sin\left[k_s(d-x)\right]+H(0)\sin(k_s x)}{k_s^2-k^2\varepsilon(k_s)}. \qquad (3.23b)$$

As one can see, the electromagnetic field distribution (3.23) restricted to the finite thickness of metallic slab, is formed by a superposition of discrete normal electromagnetic modes with quantized electromagnetic wave number k_s, Eq. (3.2). Each normal *s*-mode independently participates in the total electromagnetic response of a metal layer. The interaction of the conduction electrons with the given *s*-mode is described by its own permittivity $\varepsilon(k_s)$,

$$\varepsilon(k_s)=1-\frac{\omega_p^2}{\omega^2}\mathcal{Q}(k_s), \qquad (3.24)$$

which is not a permittivity associated with the total electromagnetic field. The dependence of $\varepsilon(k_s)$ on the mode wave number k_s, caused by both the quantum effects and the nonlocality, are incorporated into the quantum nonlocality factor $\mathcal{Q}(k_s)$ defined by

$$\mathcal{Q}(k_s)=\frac{3\omega}{4}\left(\frac{k_F d}{\pi}\right)^{-1}\sum_{n=-N_F}^{N_F\,\prime}\frac{1-q_n^2/k_F^2}{\omega-\omega_{n+|s|,n}+i\nu}. \qquad (3.25)$$

Here the prime at the sum-symbol means the absence of the term with $n=0$. The quantum nonlocality factor $\mathcal{Q}(k_s)$ and, as a consequence, the *s*-mode permittivity $\varepsilon(k_s)$ are even functions of the mode wave number,

$$\mathcal{Q}(-k_s)=\mathcal{Q}(k_s), \qquad \varepsilon(-k_s)=\varepsilon(k_s). \qquad (3.26)$$

As is ascertained below, the representation of discrete normal electromagnetic modes (3.23)–(3.25) is the most relevant and adequate in modern metallic microstructures and, especially, in nano-thin films, due to the well pronounced size effect and strong spatial dispersion.

4. Surface impedances

The external response of the metal layer to an electromagnetic excitation is completely determined by the surface impedances ζ_0 and ζ_d of the left-hand $x=0$ and right-hand $x=d$ boundaries. They are defined by the transfer relation between the respective values of the electric and magnetic fields,

$$\begin{pmatrix}E(0)\\E(d)\end{pmatrix}=\begin{pmatrix}\zeta_0 & -\zeta_d\\ \zeta_d & -\zeta_0\end{pmatrix}\begin{pmatrix}H(0)\\H(d)\end{pmatrix}. \qquad (4.1)$$

In line with the resulting formula (3.23a) for the electric field, the closed and explicit analytical expressions for the surface impedances ζ_0 and ζ_d are given by

$$\zeta_0=-\frac{ik}{d}\sum_{s=-\infty}^{\infty}\frac{1}{k_s^2-k^2\varepsilon(k_s)}, \qquad (4.2a)$$

$$\zeta_d=-\frac{ik}{d}\sum_{s=-\infty}^{\infty}\frac{\cos(k_s d)}{k_s^2-k^2\varepsilon(k_s)}. \qquad (4.2b)$$

Both impedances are composed by different electromagnetic *s*-modes characterized by their permittivities $\varepsilon(k_s)$, Eqs. (3.24), (3.25).

Within the local regime, where the spatial variation scale $|\,k_s\,|^{-1}$ of the contributive normal *s*-mode is much greater than the absolute value of the effective mean-free path of electrons $l_\omega=V_F/(\nu-i\omega)$, the transition frequency $\omega_{n+|s|,n}$ turns out to be negligible in comparison with the complex frequency $\omega+i\nu$,

$$|\,k_s l_\omega\,|\ll 1 \quad\Leftrightarrow\quad |\,\omega_{n+|s|,n}\,|\ll|\,\omega+i\nu\,|. \qquad (4.3)$$

In this case the quantum nonlocality factor $\mathcal{Q}(k_s)$ is properly described by its value $\mathcal{Q}(0)$,

$$\mathcal{Q}(0)=\frac{\omega}{\omega+i\nu}\,\mathcal{K}_{DL}^{(q)}, \qquad (4.4a)$$

$$\mathcal{K}_{DL}^{(q)}=\frac{3}{2}\frac{1}{k_F d/\pi}\sum_{n=1}^{N_F}\left[1-\left(\frac{n}{k_F d/\pi}\right)^2\right]. \qquad (4.4b)$$

In the factor $\mathcal{K}_{DL}^{(q)}$, the sum over the electron discrete quantum number n can be calculated explicitly. As a result, the

effective mode permittivity (3.24) loses the k_s-dependence and transforms into the quantum version of the local permittivity in the Drude–Lorentz model,

$$\varepsilon(0) = 1 - \frac{\omega_p^2}{\omega(\omega + i\nu)}\, \mathcal{K}_{DL}^{(q)}, \tag{4.5a}$$

$$\mathcal{K}_{DL}^{(q)} = \frac{3}{2}\frac{N_F}{k_F d/\pi}\left[1 - \frac{1}{6}\frac{(N_F+1)(2N_F+1)}{(k_F d/\pi)^2}\right]. \tag{4.5b}$$

Note that the quantum Drude–Lorentz permittivity (4.5) has a form similar to the conventional one, however, with the renormalized by the electron quantization plasma frequency: $\omega_p \to \omega_p\sqrt{\mathcal{K}_{DL}^{(q)}}$. The transition to the classical Drude–Lorentz model is realized when the number N_F of the electron conducting channels becomes sufficiently great, and there is no significant distinction between the channel parameter $k_F d/\pi$ and its integer part N_F . Therefore,

$$\varepsilon(0) \to \varepsilon_{DL} = 1 - \frac{\omega_p^2}{\omega(\omega + i\nu)} \quad \text{for} \quad k_F d/\pi \gg 1, \tag{4.6a}$$

$$\text{because} \quad \mathcal{K}_{DL}^{(q)} \to 1. \tag{4.6b}$$

Within the local regime (4.3), the summation over the mode index s in Eqs. (4.2) for the surface impedances can be explicitly performed, resulting in, see Refs. 4, 5,

$$\zeta_0^{(\mathrm{loc})} = \frac{i}{\sqrt{\varepsilon(0)}}\cot(kd\sqrt{\varepsilon(0)}), \tag{4.7a}$$

$$\zeta_d^{(\mathrm{loc})} = \frac{i/\sqrt{\varepsilon(0)}}{\sin(kd\sqrt{\varepsilon(0)})}. \tag{4.7b}$$

For thick metal slabs, surface impedances (4.7) admit the asymptotics that are well known in the theory of the normal skin effect (see, e.g., Ref. 1),

$$\zeta_0^{(\mathrm{loc})} \to 1/\sqrt{\varepsilon(0)}, \quad \zeta_d^{(\mathrm{loc})} \to 0 \quad \text{as} \quad kd\sqrt{|\,\varepsilon(0)\,|} \to \infty. \tag{4.8}$$

On the contrary, for extremely thin metal layers, both local impedances (4.7) almost compensate each other obeying asymptoitcs

$$\zeta_0^{(\mathrm{loc})} \approx \zeta_d^{(\mathrm{loc})} \to i/kd\varepsilon(0) \quad \text{for} \quad (kd)^2\,|\,\varepsilon(0)\,| \ll 1. \tag{4.9}$$

In the most relevant and significant situation when the wave frequency ω is found between the electron relaxation rate ν and the plasma frequency ω_p ,

$$\nu \ll \omega \ll \omega_p, \tag{4.10}$$

Eqs. (4.5), (4.6) for the Drude-Lorentz permittivity $\varepsilon(0)$ are simplified, and the estimations (4.8) and (4.9) for the surface impedaces take, correspondingly, simpler form,

$$\zeta_0^{(\mathrm{loc})} \to \frac{\nu - 2i\omega}{2\omega_p}, \quad \zeta_d^{(\mathrm{loc})} \to 0, \text{ if } \delta \ll d; \tag{4.11a}$$

$$\zeta_0^{(\mathrm{loc})} \approx \zeta_d^{(\mathrm{loc})} \to \frac{\delta}{d}\frac{\nu - i\omega}{\omega_p}\mathcal{K}_{DL}^{(q)\,-1}, \text{ if } d^2 \ll \delta^2. \tag{4.11b}$$

Here we introduced the minimal skin depth $\delta = c/\omega_p$ of electromagnetic field penetration in a bulk metal ($\delta \ll d$), which is reached in the high-frequency range (4.10) in the classical Drude–Lorentz model, where $\varepsilon(0) = -(\omega_p/\omega)^2$. As one can recognize, within the frequency range (4.10), all impedances (4.11) are mainly imaginary. Furthermore, the impedances (4.11b) of thin (quantum) metal layers get the value $\delta/d \gg 1$ times greater than that valid in the opposite case of thick slabs, Eq. (4.11a).

In the context of the analysis performed above, we should address a remarkable feature of the general expressions (4.2) for the surface impedances. These expressions contain the term with the electromagnetic mode index $s = 0$. It is strictly coincides with Eq. (4.9), thus, contributing to the impedance behavior of the metal thin films. Such a contribution of the only zero normal mode is spatially dispersionless independently of either the other nonzero $(s \neq 0)$ modes are local $(|\,k_s l_\omega\,| \ll 1)$ or nonlocal $(|\,k_s l_\omega\,| > 1)$. As stated above, the asymptotics Eqs. (4.9), (4.11b) defined by the term with $s = 0$, are really relevant when the nonzero modes are also spatially dispersionless, see requirement (4.3). However, as it follows from the numerical study discussed in Sec. 5, for sufficiently thin metal layers $(d < \delta)$, even in the case of strong nonlocality $(|\,k_s l_\omega\,| > 1)$ the local zero-mode can provide a noticeable contribution described by Eq. (4.11b), to the ω-dependence of the imaginary part of the surface impedances (4.2) within the high frequency range (4.10).

Our results (3.21), (3.23)–(3.25), and (4.2) give evidence that within the nonlocal quantum regime the electromagnetic response of the metal slab has resonant behavior provided by the quantization of transverse motion of the conduction electrons. Specifically, in agreement with the structure (3.25) of the quantum nonlocality factor $\mathcal{Q}(k_s)$, each nonzero $(s \neq 0)$ normal electromagnetic *s*-mode undergoes a set of quantum resonances. Due to parity (3.26) of $\mathcal{Q}(k_s)$, every given resonant set is equally contributed by two modes with indices $\pm|\,s\,|$. The resonances of the $|\,s\,|$-set occur at the values of wave frequency ω equal to the electron transition frequency $\omega_{n+|s|,n}$, Eq. (3.15),

$$\omega = \omega_{n+|s|,n}, \qquad n = 1,2,3,\ldots,N_F. \tag{4.12}$$

The number of the *s*-resonances coincides with the total number $N_F = [k_F d/\pi]$ of the electron conducting channels. In view of the restriction on the electron quantum number *n*, the frequencies (4.12) of the resonant $|\,s\,|$-set are confined to the range

$$0 < \omega - \omega_s < |\,k_s\,|\,V_F = |\,s\,|\,(\pi V_F/c)(\delta/d)\omega_p. \tag{4.13}$$

Remarkably, this is exactly the range, where the strong spatial dispersion (nonlocality) condition $|k_s l_\omega| > 1$ is met for the respective normal $\pm|s|$-modes. The width of the nonlocality interval (4.13) is determined by value of the Fermi velocity V_F of conduction electrons and, for a specific metal, is expected to become broader when the slab thickness d decreases. The higher modes with the greater $|s|$ get the wider nonlocality range and the higher threshold frequency ω_s. Due to the latter, the resonances of the $(|s|+1)$-set are always shifted to the higher frequencies with respect to the resonances of the $|s|$-set and cannot coincide with them. The resonances belonging to any fixed $|s|$-set, are equidistantly spaced inside the frequency range (4.13). Following definition (3.15), the resonant spacing $\Delta_s(d)$ reads

$$\Delta_s(d) \equiv \omega_{n+1,s} - \omega_{n,s} = |k_s| V_F (k_F d/\pi)^{-1}. \quad (4.14)$$

The spacing (4.14) of the resonant $|s|$-set with electromagnetic mode index $|s| = 2, 3, \ldots$ is a multiple of the spacing of the first set with $|s| = 1$. The resonant amplitudes of $\mathcal{Q}(k_s)$ are modulated by the factor $\omega_{n+|s|,n}(1 - q_n^2/k_F^2) \propto \propto (1 - q_n^2/k_F^2) q_n/k_F$. Therefore, the amplitudes of the lateral resonances with small and large electron quantum indices n are smaller than the amplitudes of the intermediate resonances. Evidently, the electron relaxation rate $\nu \neq 0$ broadens the resonances and decreases their amplitudes. This fact establishes the resolution condition for the resonances of the $|s|$-set constrained to the nonlocality interval (4.13),

$$\nu < \Delta_s(d). \quad (4.15)$$

In other words, the resonances satisfied condition (4.15) turn out to be well resolved.

As the electron-channel parameter $k_F d/\pi$ increases, the number N_F of $|s|$-resonances inside the frequency range (4.13) also increases, and the spacing (4.14) between them expectedly decreases. Therefore, for sufficiently great values of the electron-channel parameter $k_F d/\pi \gg 1$, the resolution condition (4.15) can be broken. As a result, the resonances of a fixed $|s|$-set begin to overlap and even to coalesce giving rise to their disappearance. In addition, the relative distance $(k_F d/\pi)^{-1}$ between the neighboring electron conducting channels becomes extremely narrow. Due to all these reasons, in definition (3.25) for $\mathcal{Q}(k_s)$, the summation over the electron quantum number n can be changed into the integration over the transverse projection $n_x = q_n/k_F = n/(k_F d/\pi)$ of the electron wave unit-vector. In such a way, the quantum nonlocality factor $\mathcal{Q}(k_s)$ achieves its classical counterpart,

$$\mathcal{Q}_B(k_s) = \frac{3\omega}{4} \int_{-1}^{1} \frac{(1 - n_x^2) dn_x}{\omega - |k_s| V_F n_x + i\nu}, \quad (4.16)$$

which does not include quantum resonances discovered above. The electromagnetic field distribution (3.23) as well as the surface impedances (4.2) contributed by the discrete normal electromagnetic s-modes with the effective mode permittivity $\varepsilon(k_s)$ described by Eq. (3.24) which, however, contains the classical nonlocality factor $\mathcal{Q}_B(k_s)$, have been obtained in Ref. 3 with the use of the method of the Boltzmann kinetic equation. Remarkably, the integrand in Eq. (4.16) possesses the famous Landau singularity, the pole at $|k_s| V_F n_x = \omega + i\nu$, which transforms to its discrete version, the resonance condition (4.12), within the quantum regime. Under the strong nonlocality (spatial dispersion), where $|k_s l_\omega| > 1$, this constitutive singularity turns out to be exactly within the integration interval, thus providing a positive imaginary part of the mode permittivity $\varepsilon(k_s)$, even in the case when the collisional relaxation rate vanishes, $\nu = 0$. As a result, the related normal $\pm|s|$-modes undergo the classical collisionless Landau damping (see, details in Refs. 3, 5). The condition $|k_s l_\omega| > 1$ of the strong nonlocality clearly attests: The frequency range, where the Landau damping appears in the electromagnetic response of two fixed normal $\pm|s|$-modes, coincides with the frequency range (4.13) of the corresponding resonant $|s|$-set (remember that the recoil frequency ω_s should be omitted in the classical limit). Hereby, in the quantum nonlocal regime (4.13), the Landau damping manifests itself as the $|s|$-set of resonances, which coalesce in the classical nonlocality and, in this way, shape the conventional Landau damping.

With increase of the wave frequency ω, the effective mean-free path of electrons l_ω decreases, and the transition to the local regime (4.3) is realized. The Landau damping vanishes since the classical nonlocality factor (4.16) approaches its asymptotics

$$\mathcal{Q}_B(k_s) \to \mathcal{Q}_B(0) = \mathcal{Q}_{DL} \equiv \frac{\omega}{\omega + i\nu} \quad \text{for} \quad |k_s l_\omega| \ll 1. \quad (4.17)$$

This conclusion is in agreement with that follows from the classical Drude–Lorentz model, compare Eqs. (3.24), (4.17) with Eqs. (4.4), (4.6).

5. Numerical results

Here we present the results of our numerical calculations of the surface impedances, derived analytically in the previous section, in order to analyze their behavior in both quantum and classical regimes. Specifically, Figs. 2–5 show the frequency spectra of the real and imaginary parts of the surface impedances, $\zeta_0(\omega/\omega_p)$ and $\zeta_d(\omega/\omega_p)$, of silver (Ag) slabs with different normalized thicknesses d/δ. In the calculations, we use an electron relaxation rate $\nu = 2.0 \cdot 10^{-4} \omega_p$, which can be quite realistic for high-quality silver films [22–24], even at room temperature.

Each panel of Figs. 2 and 3 for the real parts of the surface impedances, $\mathrm{Re}\zeta_0$ and $\mathrm{Re}\zeta_d$, displays a family of four curves. Two of them, dot-dashed green and dotted pink curves, were obtained within the quantum local approach and

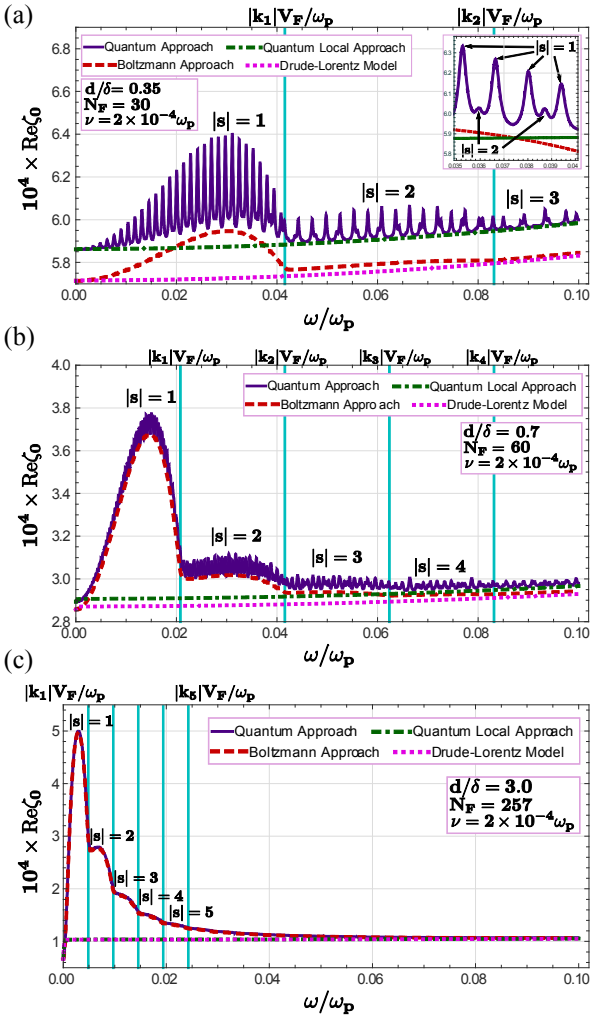

Fig. 2. (Color online) Frequency dependence of the real part of the surface impedance ζ_0 of a silver slab ($V_F = 1.39\cdot10^8$ cm/s, $\omega_p = 2.175\cdot10^3$ THz [22]) predicted by four distinct models. Each panel corresponds to a different value of the layer thickness d (marked in the panels). The electron relaxation rate $\nu = 2.0\cdot10^{-4}\,\omega_p$.

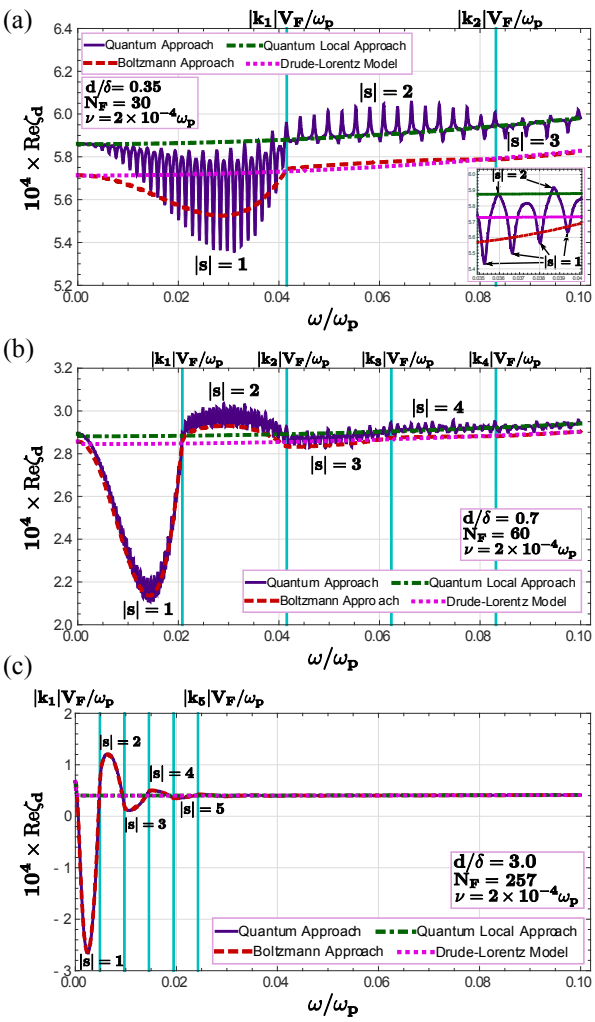

Fig. 3. (Color online) Frequency dependence of the real part of the surface impedance ζ_d at the right boundary $x = d$ of a silver slab. The curves in panels (a), (b), and (c) were calculated for the same values of the slab thickness d as in the respective panels of Fig. 2.

classical local Drude–Lorentz model, i.e., by using Eqs. (4.7) with the dielectric permittivity $\varepsilon(0)$ taken from Eqs. (4.5) and (4.6), respectively. The dashed red curves depict the frequency dependence of the real part of surface impedances obtained within the kinetic Boltzmann equation approach, where the dominant effect is the Landau damping. Here, following Refs. 3, 5, we have applied the general expressions (4.2) for the surface impedances complemented by the effective mode permittivity (3.24) with the classical nonlocality factor $\mathcal{Q}_B(k_s)$, Eq. (4.16). The real parts of the quantum nonlocal surface impedances are presented by the solid purple curves. The later results were obtained by two ways. The first one consists in numerically solving the initial system, Eqs. (3.3), (3.7), (3.21) and (4.1), while the second one is based on the examination of analytical results (4.2), (3.24) and (3.25). Both methods reveal an excellent mutual agreement. The vertical blue straight lines denote the right border of Eq. (4.13), to the right of which the corresponding normal modes of given $|s|$ quit contributing to quantum/classical nonlocality. As a consequence, the maximal/minimal value of the curves is achieved to the left from the $|k_1|V_F/\omega_p$ line, where all the $s \neq 0$ normal modes contribute to the surface impedance.

Panels (a) of Figs. 2 and 3 exhibit the spectra of $\mathrm{Re}\zeta_0(\omega/\omega_p)$ and $\mathrm{Re}\zeta_d(\omega/\omega_p)$ for nano-thin metal layers with $d/\delta = 0.35$. In this case the number of quantum electron conducting channels is moderate, $N_F = [k_F d/\pi] = 30$ and the frequency range (4.13) of nonlocality is wide enough to allow the fulfillment of the resolution condition (4.15): $\nu < \Delta_s(d) \approx 1.4\cdot10^{-3}\,|s|\,\omega_p$ for all the nonzero normal electromagnetic $|s|$-modes. Consequently, the quantum regime is clearly realized. The spectrum of the real part of the surface impedances (solid purple curves) contains well-pronounced resonances and drastically differs from the real part of the nonlocal surface impedances (dashed red curves) provided by the classical Landau damping [3,5]. It is noteworthy that inside the frequency range $0 < \omega - \omega_1 < k_1 V_F =$

$= \pi V_F / d$, where the prevailing resonances belong to the normal modes with $|s| = 1$, the resonance set with $|s| = 2$ also gives an unusual contribution: While the maxima (minima) of the resonant oscillations of $\mathrm{Re}\zeta_0$ ($\mathrm{Re}\zeta_d$) come from the $|s| = 1$ resonances, the minima (maxima) are, in fact, modulated by the $|s| = 2$ resonances, see the insets of panels. Moreover, Fig. 2 reveals that inside each nonlocality range (4.13), the resonance condition (4.12) for respective normal $|s|$-modes always gives rise to the maxima of the resonant oscillations of $\mathrm{Re}\zeta_0$. In contrast, as can be seen from Fig. 3, the resonances (4.12) in odd (even) normal $|s|$-modes determine, respectively, the minima (maxima) of the $\mathrm{Re}\zeta_d$ curve within the corresponding nonlocality intervals. The reason is the sign-alternating factor $\cos(k_s d) = (-1)^{|s|}$ present in the summands of definition (4.2b) for the surface impedance ζ_d, whereas such a factor is absent in definition (4.2a) for the other impedance ζ_0.

The intermediate situation between quantum and classical regimes is shown in panels (b), where $d/\delta = 0.7$ and $N_F = 60$. This case is close to the resolution limit $\nu = \Delta_1(d)$ for the resonant ($|s| = 1$)-set, which is achieved when the slab thickness $d \sim \delta$. Then, the resonances with $|s| = 1$ have almost coalesced. As a consequence, the quantum (solid purple) and the classical nonlocal (dashed red) curves have almost merged inside the interval $0 < \omega - \omega_1 < k_1 V_F$. On the other hand, the resonances of the sets with the electromagnetic mode indices $|s| = 2$ and $|s| = 3$ are still observed because they have a resonant spacing (4.14), respectively, two and three times larger than that for resonances with $|s| = 1$.

Surface impedances in panels (c) have been calculated for a relatively-thick slab ($d/\delta = 3$), having a very large number of electron conducting channels ($N_F = 257$). For this reason, the set of resonances cannot be distinguished for

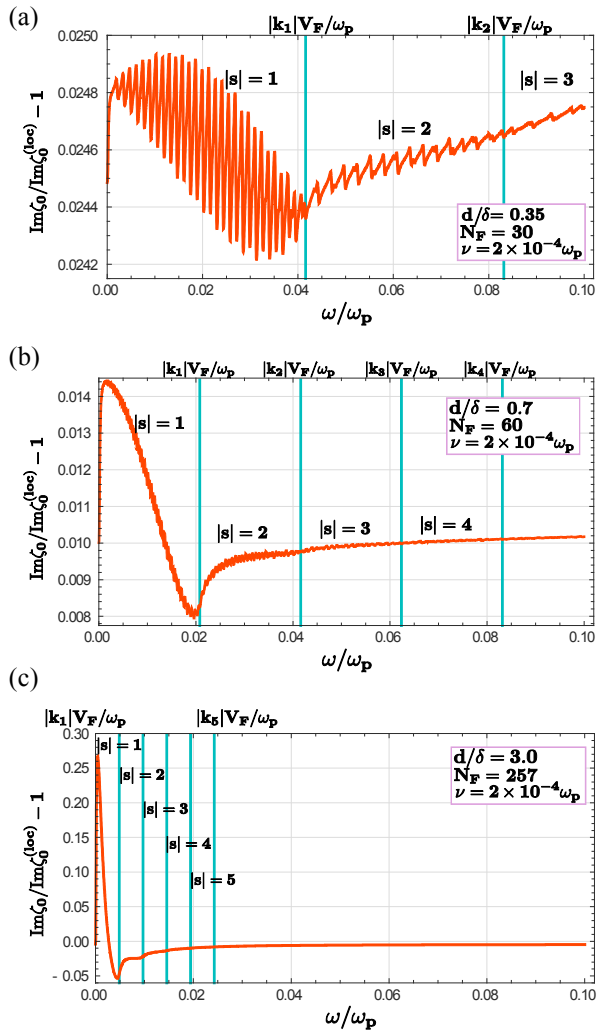

Fig. 4. (Color online) Frequency dependence of the relative difference between the imaginary parts of the nonlocal and local surface impedances at the left boundary $x = 0$ of a silver slab. The curves in panels (a), (b), and (c) were calculated with the same values for the slab thickness d as in the respective panels of Fig. 2.

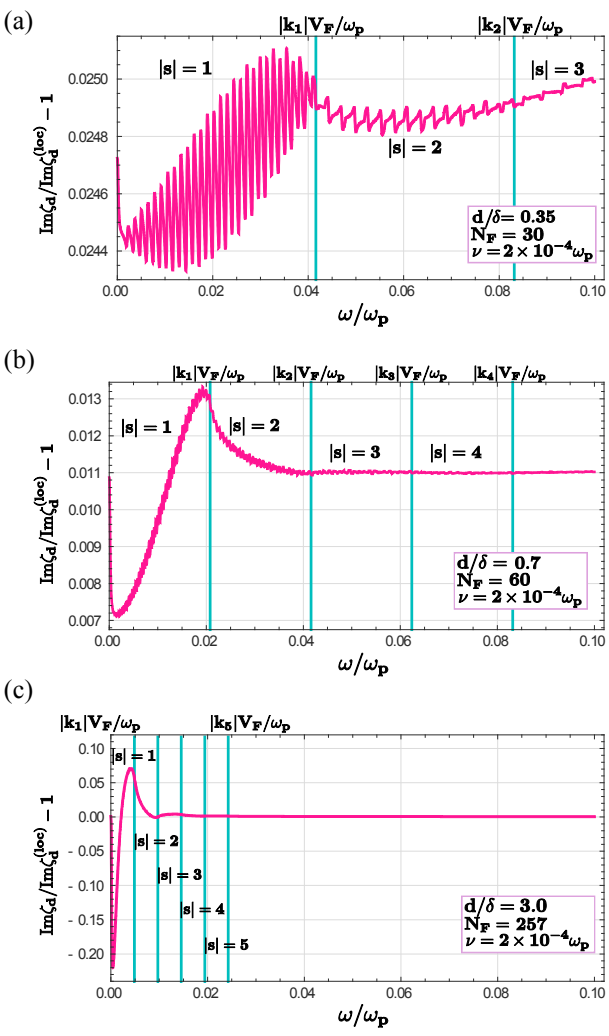

Fig. 5. (Color online) Frequency dependence of the relative difference between the imaginary parts of the nonlocal and local surface impedances at the right boundary $x = d$ of a silver slab. The curves in panels (a), (b), and (c) were calculated with the same values for the slab thickness d as in the respective panels of Fig. 2.

the first normal modes with $|s| \leqslant 10$, for which the spacing $\Delta_s(d = 3\delta) < \nu$. Here the frequency dependence of the surface impedances is determined by the classical nonlocal Landau damping effect. The spectrum of the real part of surface impedances calculated within the quantum approach (solid purple curve) perfectly coincides with that obtained within the kinetic Boltzmann equation formalism [3].

Since the nonlocality factors, $\mathcal{Q}(k_s)$ or $\mathcal{Q}_B(k_s)$, tend to the respective asymptotics (4.4) or (4.17) with the increase of wave frequency ω, all the nonlocal (solid purple and dashed red) curves approach the corresponding (quantum or classical) Drude–Lorentz curves. As a result, the oscillations are naturally smoothed, decrease in amplitude, and disappear. On the other hand, obeying the same ω-dependence, the Drude–Lorentz quantum (dot-dashed green) and classical (dotted pink) spectral curves exhibit different values in the quantum panel (a), then come closer together in the intermediate panel (b) and, subsequently, merge in the classical panel (c) as the slab thickness d (or, the same, the number of electron conducting channels N_F) increases.

Due to the fact that the real part of surface impedances determines the electromagnetic losses in a metal, the effect of the resonant quantization of Landau damping should also manifest itself in the metal absorption spectrum $A(\omega)$. The corresponding study was reported in our previous brief letter [17]. The direct comparison of the graphical presentation given in Ref. 17 for the ω-dependence of the far-infrared absorption of metal nanoslabs, displays that the line-shape of $A(\omega)$ exactly follows the resonant line-shape of $\mathrm{Re}\zeta_0(\omega)$ discovered in Fig. 2.

Quantum Landau damping also manifests itself in the frequency dependence of the imaginary parts, $\mathrm{Im}\zeta_0$ and $\mathrm{Im}\zeta_d$, of the surface impedances (4.2). The characteristic spectra and their dynamics realized with transition from the quantum to classical nonlocal regimes (with variation of the dimensionless slab thickness d/δ) are shown in Figs. 4 and 5. As was revealed with the use of our numerical simulations, inside the high frequency range (4.10), the imaginary parts of the surface impedances of the nano-thin metal layers ($d < \delta$) possess a nonresonant term whose absolute value is great and linearly increases as the wave frequency ω increases. In accordance with what was mentioned in Sec. 4 after Eqs. (4.11), this local term originates from the contribution of the local zero-mode ($s = 0$) in the sums (4.2) and is exactly described by Eq. (4.9) having the asymptotics (4.11b). Remarkably, the same expressions are also inherent for the local impedances (4.7). Therefore, in order to eliminate such a local contribution from our analysis of the quantum nonlocal effects, in Figs. 4 and 5, we present the difference between the imaginary part of the impedance ζ_0 (ζ_d) and the imaginary part of its local counterpart $\zeta_0^{(\mathrm{loc})}$ ($\zeta_d^{(\mathrm{loc})}$) normalized to the respective imaginary part of the local impedance from Eq. (4.7).

6. Conclusions

We have derived general analytical expressions for the quantum nonlocal electron current density in a metallic nanoslab within the Kubo's linear response formalism. Using this result, we have analytically calculated the electromagnetic field distribution inside the metal nanoslab by expressing it as a superposition of discrete electromagnetic modes. To study the external response, we have obtained general explicit expressions for the surface impedances of both metal slab boundaries. It was found that the frequency dependence of the surface impedances has resonances, whose origin is owing to the discretization of the electromagnetic and electron wave numbers inside the nanoslab and is directly associated with the effect of the collisionless Landau damping in the quantum regime. The quantum nonlocal resonances are well-resolved when the thickness of the metal nanoslab is smaller than the electromagnetic skin depth. It is noteworthy that the quantum resonant behavior of the frequency dependence of the surface impedances differs completely from that observed in other regimes, namely the quantum local regime, the regime described by the semiclassical Boltzmann kinetic equation formalism, and the classical local regime described by Drude–Lorentz model. The difference is due to the discretization of the Landau damping in the quantum nonlocal regime.

Acknowledgments

This work was partially supported by the VIEP-BUAP (México) under the grant No. 100312733-VIEP2018.

1. E.A. Kaner, A.A. Krokhin, N.M. Makarov, *Spatial Dispersion and Surface Electromagnetic Absorption in metals, in the Book Spatial Dispersion in Solids and Plasmas*, P. Halevi (ed.), Elsevier, Amsterdam, vol. 1, Chap. 2, 161–214 (1992).
2. L. Landau, *J. Phys*. **10**, 25 (1946).
3. A. Paredes-Juárez, F. Díaz-Monge, N.M. Makarov, and F. Pérez-Rodríguez, *JETP Lett*. **90**, 623 (2009).
4. A. Paredes-Juárez, D.A. Iakushev, B. Flores-Desirena, N.M. Makarov, and F. Pérez-Rodríguez, *Opt. Express* **22**, 7581 (2014).
5. A. Paredes-Juárez, D.A. Iakushev, B. Flores-Desirena, N.M. Makarov, and F. Pérez-Rodríguez, *Opt. Lett.* **40**, 3588 (2015).
6. F. Díaz-Monge, A. Paredes-Juárez, D.A. Iakushev, N.M. Makarov, and F. Pérez-Rodríguez, *Opt. Mater. Express* **5**, 361 (2015).
7. X. Li, D. Xiao, and Z. Zhang, *New J. Phys.* **15**, 023011 (2013).
8. S. Raza, S.I. Bozhevolnyi, M. Wubs, and N.A. Mortensen, *J. Phys.: Condens. Matter* **27**, 183204 (2015).
9. N.A. Mortensen, S. Raza, M. Wubs, T. Søndergaard, and S.I. Bozhevolnyi, *Nat. Commun*. **5**, 3809 (2014).
10. T.V. Shahbazyan, *Phys. Rev. B* **94**, 235431 (2016).

11. A.S. Kirakosyan, M.I. Stockman, and T.V Shahbazyan, *Phys. Rev. B* **94**, 155429 (2016).
12. A. Brandstetter-Kunc, G. Weick, C.A. Downing, D. Weinmann, and R.A. Jalabert, *Phys. Rev. B* **94**, 205432 (2016).
13. A. Vagov, I.A. Larkin, M.D. Croitoru, and V.M. Axt, *Phys. Rev. B* **93**, 195414 (2016).
14. A.A. Yushkanov and N.V. Zverev, *Phys. Lett. A* **381**, 679 (2017).
15. N.V. Zverev and A.A. Yushkanov, *Opt. Spectrosc.* **122**, 202 (2017).
16. J. Khurgin, W.-Y. Tsai, D.P. Tsai, and G. Sun, *ACS Photonics* **4**, 2871 (2017).
17. S.G. Castillo-López, N.M. Makarov, and F. Pérez-Rodríguez, *Opt. Lett.* **43**, 2410 (2018).
18. R. Kubo, *J. Phys. Soc. Japan* **12**, 570 (1957).
19. A.A. Abrikosov and I.A. Ryzhkin, *Adv. Phys.* **27**, 147 (1978).
20. K.B. Efetov, *Adv. Phys.* **32**, 53 (1983).
21. O.V. Konstantinov and V.I. Perel, *Sov. Phys. JETP* **10**, 560 (1960).
22. M.A. Ordal, L.L. Long, R.J. Bell, S.E. Bell, R.R. Bell, R.W. Alexander, Jr., and C.A. Ward, *Appl. Opt.* **22**, 7 (1983).
23. P. Markoš and C.M. Soukoulis, *Wave Propagation. From Electrons to Photonic Crystals and Left-Handed Materials*, Princeton University Press, Princeton, NJ (2008).
24. Y. Wu, C. Zhang, N.M. Estakhri, Y. Zhao, J. Kim, M. Zhang, X.-X. Liu, G.K. Pribil, A. Alu, C.-K. Shih, and X. Li, *Adv. Mater.* **26**, 6106 (2014).

Квантова дискретизація поглинання Ландау

S.G. Castillo-López, F. Pérez-Rodríguez, Н.М. Макаров

Отримано та проаналізовано аналітичні вирази для квантової густини електронного струму, а також для розподілу електромагнітного поля всередині металевої нанопластини. Виведено загальні точні вирази для поверхневих імпедансів обох границь металевої пластини. Показано, що явище беззіштовхувального поглинання Ландау виникає в частотній залежності поверхневих імпедансів у вигляді резонансів, пов'язаних з дискретизацією електромагнітних та електронних хвильових чисел всередині металевої нанопластини. Встановлено, що квантові нелокальні резонанси поверхневих імпедансів добре помітні при товщинах пластини, менших глибини електромагнітного скін-шару. Передбачена поведінка поверхневих імпедансів в квантовому нелокальному режимі радикальним чином відрізняється від такої, що проявляється в квантовому локальному наближенні, в напівкласичному підході кінетичного рівняння Больцмана, а також в класичній локальній моделі Друде–Лоренца. Аналітичне дослідження повністю узгоджується з відповідними числовими обчисленнями.

Ключові слова: просторова дисперсія, поглинання Ландау, металеві наноструктури, оптичні властивості.

Квантовая дискретизация поглощения Ландау

S.G. Castillo-López, F. Pérez-Rodríguez, Н.М. Макаров

Получены и проанализированы аналитические выражения для квантовой плотности электронного тока, а также для распределения электромагнитного поля внутри металлической нанопластины. Выведены общие точные выражения для поверхностных импедансов обеих границ металлической пластины. Показано, что явление бесстолкновительного поглощения Ландау возникает в частотной зависимости поверхностных импедансов в виде резонансов, связанных с дискретизацией электромагнитных и электронных волновых чисел внутри металлической нанопластины. Установлено, что квантовые нелокальные резонансы поверхностных импедансов хорошо различимы при толщинах пластины, меньших глубины электромагнитного скин-слоя. Предсказанное поведение поверхностных импедансов в квантовом нелокальном режиме радикальным образом отличается от того, которое проявляется в квантовом локальном приближении, в полуклассическом подходе кинетического уравнения Больцмана, а также в классической локальной модели Друде–Лоренца. Аналитическое исследование полностью согласуется с соответствующими численными рассчетами.

Ключевые слова: пространственная дисперсия, поглощение Ландау, металлические наноструктуры, оптические свойства.